



## Synchrony & Chaos in Patchy Ecosystems

R. M. HILLARY\*

Renewable Resources Assessment Group,  
Department of Environmental Science and Technology,  
Imperial College,  
London SW7 2BP,  
UK

*E-mail:* r.hillary@imperial.ac.uk

M. A. BEES

Department of Mathematics,  
University of Glasgow,  
Glasgow G12 8QW,  
UK

The apparent synchronisation of spatially discrete populations is a well documented phenomenon. However, it is not clear what the governing mechanisms are for this synchrony, and whether they are robust over a range of environmental conditions and patch specific population dynamic behaviours. In this paper, we explore two (possibly interacting) modes of coupling, and investigate their theoretically discernible, and perhaps even experimentally measurable, signatures. To aid us in this investigation we employ a planktonic example system, with direct application to plankton patchiness. Furthermore, we address the role of chaos in complex spatio-temporal dynamics; we find that chaos associated with funnel attractors can play a distinguished role, over dynamics less sensitive to small variations, in being more susceptible to generalised synchronisation (such as phase synchronisation) in the presence of small local parameter variation. This is in contrast to the case for coupled systems with identical dynamics, and suggests that non-identically coupled systems are more vulnerable to global extinction events when exhibiting funnel-type chaotic dynamics.

© 2004 Society for Mathematical Biology. Published by Elsevier Ltd. All rights reserved.

### 1. INTRODUCTION

There are myriad examples of ecosystems where there are well defined individual habitats that may also be weakly interconnected. From fish stocks to humans, factors such as migration, resource availability and environmental effects link these discrete habitats in a number of different ways. This weak coupling between population patches can cause the various patch dynamics to behave in a spatially coherent fashion, as if they are synchronised. One of the most popular examples

---

\* Author to whom correspondence should be addressed.

of such behaviour is the Canadian Hare–Lynx data set (Keith, 1963; Blasius and Stone, 2000a), where the individual population amplitudes evolve chaotically yet have almost exactly the same phase. This is not an uncommon phenomenon. For instance, evidence for population synchrony has been observed in recruiting plaice stocks around the British Isles (Fox *et al.*, 2002) and fluctuations in sheep populations, located on separate islands (Grenfell *et al.*, 1998). The Moran effect has been suggested as a possible explanation of some cases of observed population synchrony (Moran, 1953; Hudson and Cattadori, 1999; Blasius and Stone, 2000b). As a simple example, consider a system of identical linear, autoregressive systems, each with an additive stochastic forcing term. The Moran effect occurs when the asymptotic spatial correlation between the population abundance variables is equal to the spatial correlation between the associated stochastic terms. Essentially, strongly (spatially) correlated noise will eventually give rise to strongly synchronised dynamics, while spatially independent noise terms will cause the collective dynamics to appear unrelated. Later on we will see that, for the case of indirect coupling, there is a non-linear synchronising mechanism conceptually similar to the Moran effect.

One of the aims of this paper is to clarify the nature of the various mechanisms which are likely to be causing the observed synchrony. In patchy ecosystems, the coupling between habitats can be direct (due to migration or mixing) or indirect (via external environmental factors, such as the weather) or a mixture of the two. For directly coupled patches, the individual populations exert an effect on each other. On the other hand, indirect coupling due to temperature fluctuations, for example, may act over large spatial scales and so affect equally each patch. In this case, the individual populations are unlikely to exert a discernible influence on the temperature/climate. Climatic effects and migration/mixing are two of the main candidate mechanisms for population synchrony but, as in Fox *et al.* (2002), it is sometimes difficult to tell which process is principally responsible if significant mixing occurs together with a measure of correlation between the populations and environmental effects.

Using as an example a three-component model for the dynamics of nitrogen, phytoplankton and zooplankton, first developed by Steele and Henderson (1981), we shall investigate the two synchronising mechanisms in associated coupled patch systems. Furthermore, we shall demonstrate methods for calculating the boundaries of the synchronous types of behaviour in such systems and discuss the pertinent question of how one can possibly distinguish one mechanism from the other; we discuss how this may be achieved in practice.

If one allows for small, local variations in the underlying patch dynamics, a much richer array of synchronised behaviour can be observed (Pikovsky *et al.*, 1997), as has been observed in biological time series, such as the Canadian Hare–Lynx data set. We shall provide an example of one of these more relaxed forms of general synchronous behaviour and illustrate how to calculate the regions in the coupling parameter space for which the patch-to-patch relationship is smooth.

Most, if not all, predator–prey-type models are inherently non-linear and there is significant evidence for the presence of chaos both in theoretical population models (Hastings and Powell, 1991; Edwards and Brindley, 1996; Edwards and Bees, 2001) and in Nature [diatom communities Sugihara and May (1990), and in the aforementioned Canadian Hare–Lynx data]. Previous work on the role of chaos in meta-population dynamics [e.g., Allen *et al.* (1993)] was concerned with diffusively coupled, identical Ricker and logistic maps. Therein, it was observed that the desynchronising influence of chaotic dynamics allowed for a higher probability of global survival, in response to global perturbations, compared with non-chaotic dynamics. In this paper, we find that the opposite of this is true when we allow for variations in the local dynamics, for two structurally different example systems. Moreover, chaos from a common type of attractor in ecological models aids the formation of a smooth collective relationship for lower coupling values than for non-chaotic dynamics.

In the following section we shall introduce the generic forms for the two distinct (general) models of patchy, coupled ecosystems. Furthermore, we shall outline the structure of the paper.

## 2. MODELLING THE DYNAMICS OF PATCHY ECOSYSTEMS

In this paper, we work with two general classes of dynamical, coupled patch models. Although it is quite likely that both direct and indirect patch coupling will both be present, for the sake of clarity we model the two separately. However, to contrast the two classes we shall discuss them concurrently.

For the case of indirect/external coupling, the general model can be formulated in terms of a *drive system* (the external forcing factors,  $\mathbf{E}$ ) and a *response system* (the  $m$  patch inhabitants, given by the  $m$ -vector  $\mathbf{s}_i$ , for each patch  $i = 1, \dots, n$ ) as follows:

$$\begin{aligned}\dot{\mathbf{E}} &= \mathbf{F}(\mathbf{E}), \\ \dot{\mathbf{s}}_i &= \mathbf{G}(\mathbf{s}_i, \Theta, \mathbf{E}).\end{aligned}\tag{1}$$

The functions  $\mathbf{F}(\cdot)$  and  $\mathbf{G}(\cdot)$  denote the dynamics of the external forcing and the patch inhabitants, respectively. The coupling between the drive,  $\mathbf{E}$ , and response,  $\mathbf{s}_i$ , systems is characterised by the parameter vector  $\Theta$ .

The second case we shall consider is that where the patches interact directly with each other. For this particular scenario, the following general model is appropriate:

$$\dot{\mathbf{S}} = \mathbf{G}(\mathbf{S}) + \mathcal{E}_L \otimes \mathbf{H}(\mathbf{S}),\tag{2}$$

where  $\otimes$  is the direct product. Here,  $\mathbf{S} = (\mathbf{s}_1, \mathbf{s}_2, \dots, \mathbf{s}_n)^T$  represents the species present (again the  $\mathbf{s}_i$  are  $m$ -dimensional vectors and  $i = 1, \dots, n$

denotes the lattice point). The reaction dynamics is governed by the function  $\mathbf{G}(\mathbf{S}) = (\mathbf{G}(\mathbf{s}_1), \mathbf{G}(\mathbf{s}_2), \dots, \mathbf{G}(\mathbf{s}_n))^T$ . The function  $\mathbf{H}$  is an as yet arbitrary (assumed  $C^1$ ) function defined similarly in action to  $\mathbf{G}(\mathbf{S})$  and  $\mathbf{H}(\mathbf{S}) = (\mathbf{H}(\mathbf{s}_1), \mathbf{H}(\mathbf{s}_2), \dots, \mathbf{H}(\mathbf{s}_n))^T$ . This function  $\mathbf{H}$  encompasses both the nature of the coupling (linear/non-linear) and determines which patch species will be coupled to similar/different species in the other patches in the lattice. The  $n \times n$  coupling matrix  $\mathcal{E}_L$  can take many forms, depending on the coupling structure of the system concerned. One fairly common example, and the situation we consider in this paper, is that of nearest-neighbour coupling in a non-ring form (akin to a discretised reaction–diffusion system with no flux, as opposed to periodic, boundary conditions). The coupling matrix would then be defined as

$$\mathcal{E}_L = \begin{pmatrix} -\epsilon_2 & \epsilon_2 & 0 & \dots & 0 \\ \epsilon_1 & -(\epsilon_1 + \epsilon_3) & \epsilon_3 & \dots & 0 \\ \vdots & \vdots & \vdots & \vdots & \vdots \\ 0 & \dots & 0 & \epsilon_{n-1} & -\epsilon_{n-1} \end{pmatrix}, \quad (3)$$

and the corresponding coupling function  $\mathbf{H}$  would be the  $m$ -dimensional identity matrix (i.e., no cross-species coupling between patches).

Coupled oscillators, in a system such as (2), are well known to exhibit synchronisation (Fujisaka and Yamada, 1983; Pikovsky, 1984; Pecora and Carroll, 1990). Other phenomena, such as complex attracting basins and basin boundaries (Alexander *et al.*, 1992; Ott and Sommerer, 1994) and high sensitivity to low levels of system noise (Ashwin *et al.*, 1994), have also been documented and are generic features of coupled oscillators.

In the following two sections, the mechanisms behind the transition from unsynchronised to synchronised populations are discussed, for each patch model when the individual patch dynamics are chaotic. In Section 5, the effect of slight differences in the individual reaction systems is investigated; such systems may explain many of the examples of near-synchronous dynamics observed in nature, particularly strong phase similarity in population oscillations. Finally, in Section 6, the role of chaos in meta-population dynamics is explored. We find that chaos can aid *generalised* synchronisation of the patch dynamics, contrary to intuitive notions of chaos.

### 3. DIRECTLY COUPLED PATCH SYNCHRONISATION

This work was inspired by the investigation of interacting planktonic populations as coupled oscillators with application to patchy dynamics (Hillary, 2003; Hillary and Bees, 2004). With this in mind, we will employ, as an example, a three-component nutrient–phytoplankton–zooplankton (NPZ) model to represent the individual patch dynamics,  $\mathbf{G}(\cdot)$ :

Table 1. A brief explanation of model parameters and default parameter values for the NPZ<sup>I</sup> model in (4).

Parameter	Symbol	Default value
Phytoplankton growth rate	$a$	$0.2 \text{ (m day)}^{-1}$
Light attenuation by water	$b$	$0.2 \text{ m}^{-1}$
Light attenuation by phytoplankton	$c$	$0.4 \text{ m}^2 \text{ (g C)}^{-1}$
Higher predation of zooplankton	$d$	$0.142 \text{ g C m}^{-3} \text{ day}^{-1}$
Nutrient half-saturation constant	$e$	$0.03 \text{ g C m}^{-3}$
Cross-thermocline exchange rate	$k$	$0.05 \text{ day}^{-1}$
Phytoplankton respiration	$r$	$0.15 \text{ day}^{-1}$
Phytoplankton sinking	$s$	$0.04 \text{ day}^{-1}$
Lower mixed level nutrient concentration	$N_0$	$1 \text{ g C m}^{-3}$
Zooplankton growth efficiency	$\alpha$	0.25
Zooplankton excretion fraction	$\beta$	0.33
Regeneration of zooplankton excretion	$\gamma$	0.5
Zooplankton grazing rate	$\lambda$	$0.6 \text{ day}^{-1}$
Zooplankton half-saturation constant	$\mu$	$0.035 \text{ g C m}^{-3}$
Patch to patch flux	$\epsilon_i$	Bifurcation parameter

$$\begin{aligned}
 \frac{dN}{dt} &= -\frac{Na}{(e+N)(b+cP)}P + rP + \frac{\lambda\beta P^2}{\mu^2 + P^2}Z + \gamma dZ^p + k(N_0 - N), \\
 \frac{dP}{dt} &= \frac{Na}{(e+N)(b+cP)}P - rP - \frac{\lambda P^2}{\mu^2 + P^2}Z - (s+k)P, \\
 \frac{dZ}{dt} &= \frac{\alpha\lambda P^2}{\mu^2 + P^2}Z - dZ^p.
 \end{aligned} \tag{4}$$

Steele and Henderson (1981) first proposed the structure of the model. Briefly, phytoplankton grow (limited by nutrient and available light) and are lost via a combined respiration and natural mortality term ( $r$ ; recycled into nutrient), sinking ( $s$ ), exchange with phytoplankton-free deep water ( $k$ ) and grazing by zooplankton (Holling type III). Additionally, there is a source of nutrients from mixing with nutrient laden ( $N_0$ ) deep water and the system is closed by a higher predation term ( $dZ^p$ ). The bifurcational structure was investigated by Edwards and Brindley (1996) and further advanced with  $1 \leq p \leq 2$  by Edwards and Bees (2001). For a thorough review of the parameters in the model see Table 1 and the above references. The model exhibits stable equilibria, limit cycles and chaos (via the period-doubling route) under variation of the closure/higher predation rate  $d$ . In this section, we will assume that  $p = 1$ , and discuss the quadratic closure model in Section 6. This particular model was specifically formulated to model planktonic dynamics but serves equally well as a representative model of a nutrient–prey–predator system. One of the simplest coupled systems that one can envisage is just two patches, coupled via a small diffusive (e.g., swimming diffusivity of magnitude  $\epsilon = \epsilon_1 = \epsilon_2$ ) term in the predator (zooplankton) dynamics.

Throughout the remainder of this paper, we will refer to different incarnations of the above model and coupling structures to demonstrate various phenomena. To try to keep these switches in models clear, we propose the following coupled system nomenclature. The model denoted by  $\text{NPZ}_{j,=}^i$  refers to the system with underlying dynamics given by the index  $i$  (where  $i = l$  for the linear closure model;  $i = q$  for the quadratic case);  $j$  is the number of coupled patches; and the final index,  $=$  or  $\neq$ , tells us whether the coupled systems are identical ( $=$ ), or if there are local parameter variations in the underlying dynamics ( $\neq$ ). For example, the model denoted by  $\text{NPZ}_{10,=}^l$  comprises ten, identically coupled, linear closure NPZ systems.

In general, the patches are assumed to evolve chaotically and independently (for differing initial conditions) when  $\epsilon_i = 0, \forall i$ . The synchronisation set  $M_S$ , defined by

$$M_S = \{\mathbf{s}_1, \mathbf{s}_2, \dots, \mathbf{s}_n | \mathbf{s}_1(t) = \mathbf{s}_2(t) = \dots = \mathbf{s}_n(t)\}, \quad (5)$$

is where the synchronised state, denoted by  $A$ , resides (and, for the NPZ example,  $\mathbf{s}_i = (N_i, P_i, Z_i)$ ). The synchronised state will be stable if the Lyapunov exponents (Eckmann and Ruelle, 1985) transverse to  $M_S$  are negative. These *normal* exponents (Fujisaka and Yamada, 1983) are defined in the following manner. The normal Lyapunov exponent,  $\lambda_{\perp}(x, \mathbf{v})$ , from the point  $x \in A$  in the direction  $\mathbf{v} \in (T_x M_S)^{\perp}$ , is given by

$$\lambda_{\perp}(x, \mathbf{v}) = \lim_{T \rightarrow \infty} \frac{1}{T} \int_0^T \ln \left\| \prod_{(T_x M_S)^{\perp}} \circ DG^t(\mathbf{v}) \right\| dt, \quad (6)$$

where  $DG^t(\cdot)$  is the Jacobian of  $\mathbf{G}(\cdot)$  at time  $t$  and  $\prod_V$  denotes an orthogonal projection onto the vector space  $V$ . In essence, these exponents measure the exponential growth rate of transverse perturbations to the synchronous state. If we let  $\lambda_{\perp}^{\max}$  denote the largest of the exponents then any transverse perturbations grow in the manner of  $\exp(\lambda_{\perp}^{\max} t)$ . Consequently, if  $\lambda_{\perp}^{\max} < 0$  then the synchronised state will be stable to small perturbations. Under the reasonable assumption that  $A$  is an *ergodic* attractor (Eckmann and Ruelle, 1985), the expression in (6) will converge to a finite set of values that are independent of the choice of  $x \in A$ .

For the example  $\text{NPZ}_{2,=}^l$  system, we plot the coupling parameter  $\epsilon$  against the largest normal exponent  $\lambda_{\perp}^{\max}$  in Fig. 1. It can be seen that, from  $\epsilon = 0$  up to around  $\epsilon = 0.002$ ,  $\lambda_{\perp}^{\max} > 0$  (for the most part), whence the synchronised state will not be attracting. After this point however, the coupling is strong enough that  $A$  will attract a positive measure set of nearby initial conditions. The change in the stability of  $A$  is termed a *blowout* bifurcation (Ott and Sommerer, 1994). Other factors can influence the stability of the synchronous behaviour, such as noise (Alexander *et al.*, 1992; Ashwin *et al.*, 1994).

The difference of the synchronised and unsynchronised dynamical regimes can be seen in Fig. 2 where we plot the time series of  $N_2 - N_1$ , before and after the

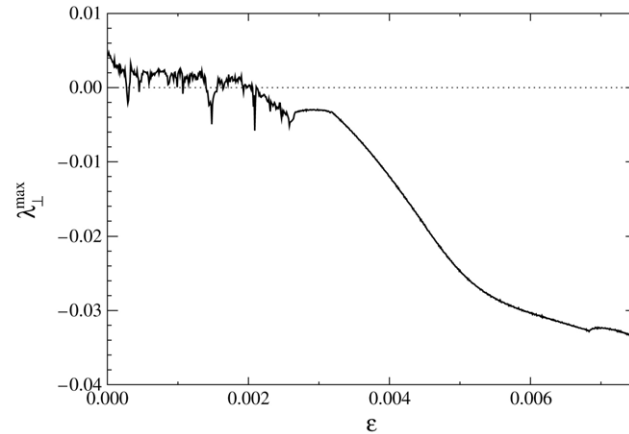


Figure 1. A plot of the maximal normal Lyapunov exponent,  $\lambda_{\perp}^{\max}$ , versus the patch coupling,  $\epsilon$ . The results shown are for the  $\text{NPZ}_{2,=}^I$  prototype two-patch systems. For  $\epsilon$  greater than approximately 0.002, the coupling is strong enough to synchronise the dynamics of the two patches.

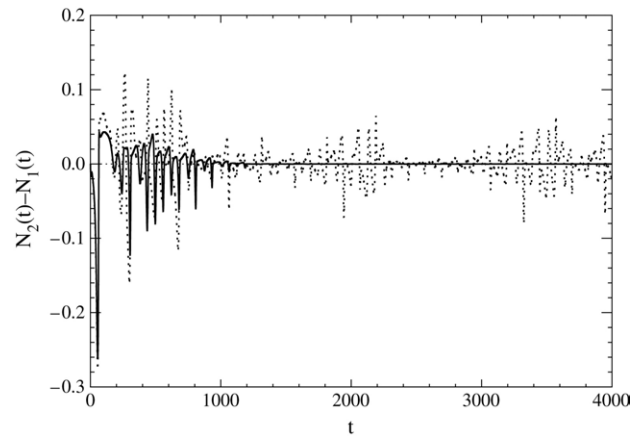


Figure 2. Time series of  $N_2 - N_1$ , for the  $\text{NPZ}_{2,=}^I$  system, after a small perturbation of the synchronised dynamics before (full line) the blowout bifurcation,  $\epsilon = 0.003$ , and after (dotted line) the blowout bifurcation,  $\epsilon = 0.001$ . Pre-blowout, we see a decay back into synchrony; post-blowout, we see the persistence of the perturbation.

blowout bifurcation, after a small, identical perturbation to the synchronised solution. Before the blowout, the perturbation dies out and the system returns to synchronicity. After the blowout, the perturbation expands exponentially (because  $\lambda_{\perp}^{\max} > 0$ ) until the growth is checked by the non-linear terms.

This phenomenon is not restricted to just two coupled patches; it was numerically observed (Hillary, 2003; Hillary and Bees, 2004) that, under certain conditions, localised coupling variations could cause a blowout bifurcation. Furthermore it was also proven that this locally initiated blowout must always result in a global

loss of stable synchronisation, for an arbitrary number of patches coupled as they are here. For more complex global coupling scenarios, such coupled arrays have been seen to exhibit cluster synchronisation (Belykh *et al.*, 2001), where some patches synchronise in discrete clusters. Also, for systems which are coupled via only one species (a migratory predator for example) it was demonstrated in Pecora (1998) that certain systems can synchronise at lower coupling and then desynchronise at higher coupling values; the extreme end of this is where there can exist an upper limit to the number of patches for which a globally synchronised state can be realised.

#### 4. INDIRECTLY COUPLED PATCH SYNCHRONISATION

We shall now address system (1), where the patches are coupled via some external forcing. For these drive–response systems, we again propose a symbolic representation:  $\text{NPZ}_{j,=}^i[E]$ , where  $i$  determines the NPZ model to be used (linear or quadratic closure, as before);  $j$  is again the number of response systems present;  $=$  or  $\neq$  describes whether the coupled systems are identical or not; and  $E$  determines the nature of the driving system. For example, the drive response system  $\text{NPZ}_{2,=}^l[\text{NPZ}^q]$  corresponds to a single, quadratic closure NPZ system, driving two equivalent linear closure NPZ systems (a case we shall consider later).

Abarbanel *et al.* (1996) investigated this type of drive–response system in order to establish a relatively simple method of detecting a deterministic relationship between the drive and the response systems when both exhibit chaotic dynamics.

The *generalised synchronisation* of chaotic drive–response systems, such as the one in (1), was thus defined to be associated with the existence of some transformation  $\phi : E \rightarrow S$  taking trajectories on the attractor in the drive space  $E$  to the attractor in response space  $S$ , i.e.,  $\mathbf{s}(t) = \phi(\mathbf{E}(t))$  [Abarbanel *et al.* (1996), see Appendix A].

On constructing an *auxiliary system* (Abarbanel *et al.*, 1996),

$$\dot{\mathbf{r}} = \mathbf{G}(\mathbf{r}, \Theta, \mathbf{E}), \quad (7)$$

which is *identical* to the original response system, the presence of generalised synchronisation can be detected. If the response and auxiliary systems are in full synchronisation [ $\mathbf{s}(t) = \mathbf{r}(t)$ ] then there exists a function  $\phi$ , with properties as defined in Appendix A, and the drive and response systems are generally synchronised.

Moreover, it seems reasonable that if the coupling between the drive and response systems is sufficiently strong (they are generally synchronised) then the response systems will be fully synchronised. Extending the analysis of Abarbanel *et al.* (1996) to an arbitrary number of response systems, we can demonstrate why this is the case. The premise begins with the assumption that if all the response systems

$(\mathbf{s}_1, \dots, \mathbf{s}_n)$  are being driven by the same driving signal,  $\mathbf{E}$ , then they will inhabit the same attractor, so long as their respective initial conditions lie in the same basin of attraction. It is possible that  $\mathbf{s}_1(t) = \mathbf{s}_2(t) = \dots = \mathbf{s}_n(t)$ , but quite unlikely if  $\mathbf{s}_1(0) \neq \mathbf{s}_2(0) \neq \dots \neq \mathbf{s}_n(0)$ , especially in the chaotic case, due to exponential separation of nearby orbits. However, if the response systems are synchronised to the drive system (via  $\phi$ ) then it is natural that the solution  $\mathbf{s}_1(t) = \mathbf{s}_2(t) = \dots = \mathbf{s}_n(t)$  occurs.

More formally, the local stability of the complex, generally synchronised oscillations,  $\mathbf{s}_i(t) = \phi(\mathbf{E}(t))$ , is equivalent to the stability of the comparatively simple regime where  $\mathbf{s}_1(t) = \dots = \mathbf{s}_n(t)$ . To see this equivalence, first consider the linearised equations for the evolution of  $\xi_i(t) = \mathbf{s}_i(t) - \phi(\mathbf{E}(t))$  and  $i = 1, \dots, n$ . We have that

$$\begin{aligned}\dot{\xi}_1 &= DG^t(\phi(\mathbf{E}), \Theta, \mathbf{E}) \cdot \xi_1, \\ \dot{\xi}_2 &= DG^t(\phi(\mathbf{E}), \Theta, \mathbf{E}) \cdot \xi_2 \\ &\quad \vdots \\ \dot{\xi}_n &= DG^t(\phi(\mathbf{E}), \Theta, \mathbf{E}) \cdot \xi_n,\end{aligned}\tag{8}$$

and  $DG^t = \partial_X \mathbf{G}(X, \Theta, \mathbf{E}(t))$  is the Jacobian matrix of  $\mathbf{G}$ , to be evaluated for the generally synchronised solution. For any  $i \neq j$ , the linear evolution of  $\xi_i(t) - \xi_j(t) = \mathbf{s}_i(t) - \mathbf{s}_j(t)$  is identical to that of  $\xi_i(t)$  and  $\xi_j(t)$ ; they have the same Jacobian matrix,  $DG^t(\phi(\mathbf{E}), \Theta, \mathbf{E})$ , as seen in (8). This now means that the linear stability of the generally synchronised motions  $\xi_i(t) = \mathbf{s}_i(t) - \phi(\mathbf{E}(t))$  in  $E \oplus S_i$  is *both* a necessary *and* a sufficient condition for the linear stability of the synchronised motions  $\mathbf{s}_i(t) = \mathbf{s}_j(t)$ , in the space  $S_1 \oplus \dots \oplus S_n$ . This result is proved in [Appendix B](#).

Consequently, for initial conditions inside the associated basin of attraction, if the external forces act strongly on the patches, the dynamics of the individual patches will become synchronised. This analysis applies to all types of dynamical behaviour, from periodic to quasi-periodic to chaotic. We also point out that the linear stability of the synchronous solution depends only on the generally synchronised solution,  $\phi(\mathbf{E}(t))$ , and the coupling parametrisation vector,  $\Theta$ . This indicates that the strength of the coupling required will be independent of the number of response systems involved; this is not true for the case of directly coupled systems ([Pecora, 1998](#)).

We give two brief numerical examples of this phenomenon: the first using the well known Rössler ([Rössler, 1976](#)) system as the external forcing field,  $\mathbf{E}$ , to represent some abstract notion of a complex, completely different field forcing the patch system—such as the weather; secondly, we employ an NPZ<sup>g</sup> model as the forcing field, to mimic some similar (in terms of timescales etc.), yet independent patch influence. In our defined terminology, the first model would be of the type NPZ<sub>2,=</sub><sup>l</sup>[Röss.], with the second defined as NPZ<sub>2,=</sub><sup>l</sup>[NPZ<sup>g</sup>]. The Rössler system

was originally designed as a model of a model in a sense and to show that chaos could spring from just one simple non-linearity:

$$\begin{aligned}\dot{x}_1 &= -(x_2 + x_3), \\ \dot{x}_2 &= x_1 + 0.2x_2, \\ \dot{x}_3 &= 0.2 + x_3(x_1 - \mu),\end{aligned}\tag{9}$$

where we choose  $\mu = 5.7$ . Our drive system is defined by  $\mathbf{E} = \mathcal{T}(\mathbf{x})$  (where  $\mathbf{x} = (x_1, x_2, x_3)$  and  $\mathcal{T}$  is a linear translation with rescaling so that, for orbits on the attractor,  $E^j \in (0, 1)$ ,  $j = 1, \dots, 3$ , as in the example  $s_i \in (0, 1)$ ). Again, for simplicity, we consider the case where only one of the drive variables is coupled to only one of the response variables; we couple the variable  $E^1$  to the equation for the nutrient evolution (to mimic a climatic influence on the nutrient) in the response systems from (4) such that

$$\dot{N}_i = \dot{s}_i^1 = G^1(s_i) + \theta(E^1 - s_i^1),\tag{10}$$

and  $\theta > 0$ . For the  $\text{NPZ}_{2,=}^l[\text{NPZ}^q]$  system, again only the nutrient evolution of the driving system is coupled to that of the response systems, as above (so as to be some representation of one-way nutrient mixing; perhaps an estuary, for example). With the drive–response structure, setting up the calculation for the Lyapunov exponents of the system is slightly more complicated than for the directly coupled systems. To easily observe how a transition from synchronised to unsynchronised dynamics can occur, based upon the driving strength, we consider the following simple quantity:

$$\zeta = \lim_{T \rightarrow \infty} \frac{1}{T} \int_0^T \|\mathbf{s}_2(t) - \mathbf{s}_1(t)\| dt.\tag{11}$$

In this limit,  $\zeta = 0$  indicates synchronised dynamics; for non-zero values of  $\zeta$ , the collective regime will be unsynchronised. For both drive–response systems,  $\text{NPZ}_{2,=}^l[\text{Röss.}]$  and  $\text{NPZ}_{2,=}^l[\text{NPZ}^q]$ , we plot in Fig. 3 the values of  $\zeta$  defined in (11), in terms of the coupling strength,  $\theta$ . In Fig. 3, we find that both drive–response systems display a transition from unsynchronised to synchronised dynamics, as  $\theta$  increases. For system  $\text{NPZ}_{2,=}^l[\text{NPZ}^q]$ , the critical value of  $\theta$  is approximately 0.08, and for system  $\text{NPZ}_{2,=}^l[\text{Röss.}]$ , the transition occurs at  $\theta \approx 0.0066$ . This disparity of the magnitudes at which the transitions occur in the different systems is due to the difference in the characteristic timescale of the driving systems. The Rössler system has a timescale of the order of days, compared to those of weeks and months in the driving and response NPZ systems. This is why the level of coupling needed in system  $\text{NPZ}_{2,=}^l[\text{Röss.}]$  to see synchronisation is much lower than that needed in system  $\text{NPZ}_{2,=}^l[\text{NPZ}^q]$ . In a colloquial sense, the ‘wrinkles’ are ‘ironed out’ faster by the driving system with the faster timescales. In Fig. 4, we plot the attractors in the  $(N_1, N_2)$  plane for the synchronised and unsynchronised cases for system  $\text{NPZ}_{2,=}^l[\text{Röss.}]$ .

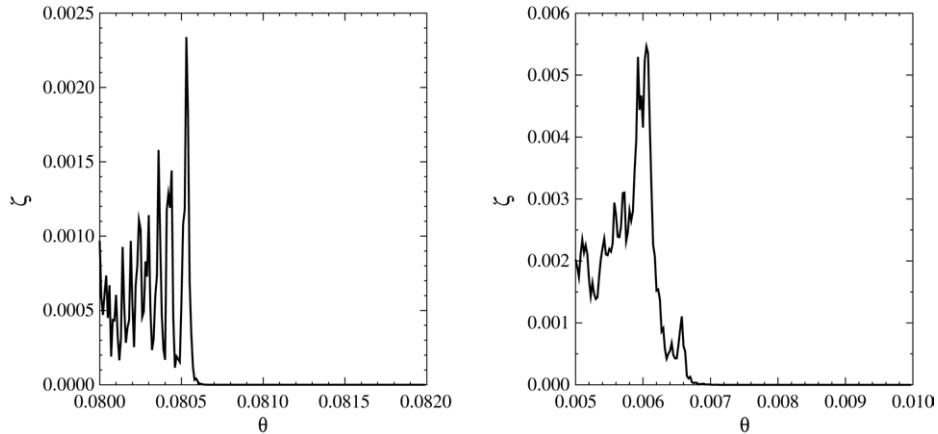


Figure 3. The mean distance from synchronisation,  $\zeta$ , in terms of the coupling strength,  $\theta$ , for (left) the drive–response systems  $\text{NPZ}_{2,=}^l$  [ $\text{NPZ}^d$ ] and (right) the drive–response system  $\text{NPZ}_{2,=}^l$  [ $\text{Röss.}$ ]. The transition from non-zero to zero values of  $\zeta$  marks the value of  $\theta$  above which we see synchronised patch dynamics in the response systems.

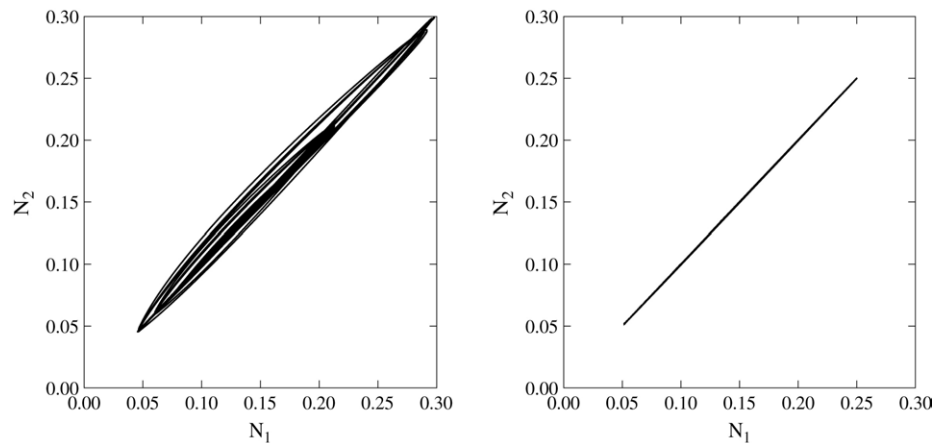


Figure 4. Attractors in the  $(N_1, N_2)$  plane for the unsynchronised (left,  $\theta = 0.001$ ) and the synchronised (right,  $\theta = 0.01$ ) motions for  $\text{NPZ}_{2,=}^l$  [ $\text{Röss.}$ ]. For both cases,  $N_1(0) \neq N_2(0)$ .

## 5. NON-IDENTICAL REACTION DYNAMICS

The general patch models in (1) and (2) assume that the individual reaction dynamics are the same but, in reality, there are likely to be some intrinsic differences between the various patches. Factors such as terrain, predatory pressure and nutrient regeneration may vary between habitats so, in general, we have some specific patch dynamics governed by  $\mathbf{G}_i(\cdot)$ . In this scenario, the patches cannot synchronise exactly, but they do exhibit a rich array of near-synchronous behaviour.

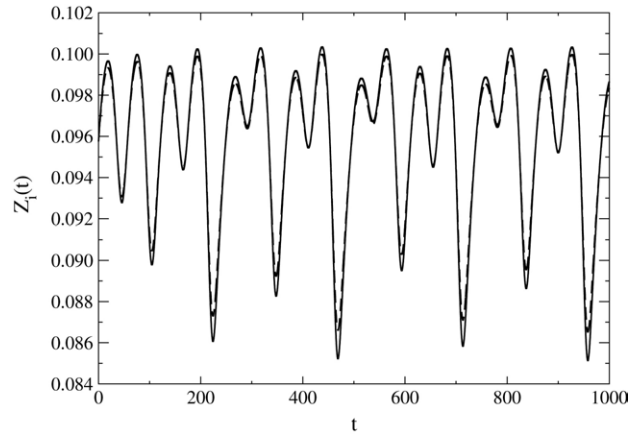


Figure 5. Phase synchronisation in the patch lattice dynamics for the patch system  $\text{NPZ}_{10,\neq}^l$ . For the example ten-patch system, we plot the time series of the variables  $Z_i$ , for  $i = 2, 5$ . Here,  $\epsilon = 0.075$ , and there is a small, time-independent stochastic variation of  $\mathcal{O}(10^{-3})$  in the closure rate  $d$ .

As an illustrative example, consider the coupled system  $\text{NPZ}_{10,\neq}^l$ , which, by our notation, defines ten patches, with non-identical dynamics, coupled together as defined in (2). In Fig. 5, we plot the time series of the predators,  $Z_i$ , from two, non-adjacent patches. To simulate habitat variations, a small, uniformly distributed stochastic perturbation,  $\chi_i$ ,  $\mathcal{O}(10^{-3})$ , was added to the patch higher predation rate,  $d_i$ , at the beginning of the simulations (but the  $d_i$ , while different, were constant throughout). For a coupling strength of  $\epsilon = 0.075$ , even though the amplitudes vary in size, the phases of the oscillations are the same. This is an example of *phase synchronisation* (Pikovsky *et al.*, 1997), and is the phenomenon observed in the Canadian Hare–Lynx data (Blasius and Stone, 2000a).

In the previous section it was demonstrated that there are threshold values of the coupling above which we see the onset of synchronised population dynamics. The same is true for the generally synchronised behaviour seen in Fig. 5, and these threshold coupling values can be computed. As an example, for a strong relationship between two generally synchronised patches, we might expect that there is some smooth function  $\Phi$  such that  $\mathbf{s}_2 = \Phi(\mathbf{s}_1)$ . This is the definition of *smooth generalised synchronisation*, and the conditions under which this can occur were described, for both directly coupled oscillators and drive–response systems, by Josic (1998). For direct coupling regimes, the results for two coupled patches (Josic, 1998) have been extended to arbitrarily many patches (Hillary and Bees, 2004).

It can be proven that the existence of the above strong relationship, for suitably small patch parameter mismatch, requires that the synchronous state  $A$  is *normally hyperbolic* (Wiggins, 1994). In essence, this means that the contraction of perturbation vectors transverse to  $M_S$  is greater than the contraction of vectors inside  $M_S$ . This can be stated in terms of the normal and standard Lyapunov exponents.

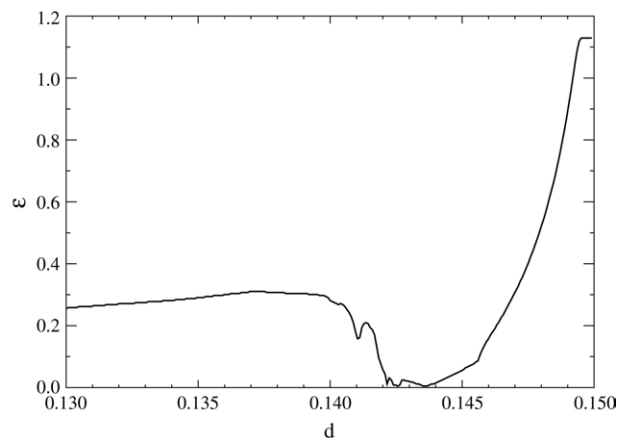


Figure 6. The neutral normal hyperbolicity curve in  $(d, \epsilon)$  space for the non-identical two-patch system  $\text{NPZ}_{2,\neq}^I$ . For values of  $\epsilon$  above the curve, and for small perturbations in the parameter  $d$ , the two patches will be (asymptotically) smoothly related via a smooth function,  $\Phi$ .

The synchronous state  $A$  is normally hyperbolic if, for all points  $x \in A$ ,  $\mathbf{v} \in T_x M_S^\perp$  and  $\mathbf{u} \in T_x M_S$ ,

$$\lambda_\perp^{\max}(x, \mathbf{v}) < \lambda_A^{\min}(x, \mathbf{u}), \quad (12)$$

where  $\lambda_\perp^{\max}$  is the maximal normal Lyapunov exponent and  $\lambda_A^{\min}$  is the smallest Lyapunov exponent of  $A$ . The function  $\Phi$  acts when all transient behaviour vanishes, taking attracting points in one patch to the corresponding points in the other patch.

As a further illustrative and simple example, we compute the boundaries of smooth collective behaviour for a two-patch system,  $\text{NPZ}_{2,\neq}^I$ , resulting from a perturbation to the underlying parameters of an  $\text{NPZ}_{2,=}^I$  system. The ideas extend to arbitrarily many patches, but both the computation and visualisation of the results and dynamics become harder as we include more patches. In Fig. 6, the strength of coupling required for  $A$  to be normally hyperbolic is plotted against the closure rate,  $d$ . This curve marks the transition from smooth to non-differentiable collective dynamics.

In Fig. 7(a) and 7(b), the dynamics of  $\text{NPZ}_{2,\neq}^I$  in the predator phase plane  $(Z_1, Z_2)$  are plotted for coupling (a) above the curve in Fig. 6 ( $\epsilon = 0.075$ ) and (b) below the curve in Fig. 6 ( $\epsilon = 0.025$ ), respectively. In both cases, there was a small initial stochastic variation in the closure rate within the chaotic regime, about  $d = 0.142$ . For the case of stronger coupling, the dynamics of the variables  $Z_1$  and  $Z_2$  are smoothly related, and in phase synchronisation; see Fig. 5. For the weaker coupling, the smoothness of the relationship is lost, because the coupling is below the normal hyperbolicity curve in Fig. 6, if a deterministic relationship still exists at all. The neutral normal hyperbolicity curve defines where the transition from smooth to non-smooth generalised synchronisation occurs, but actually

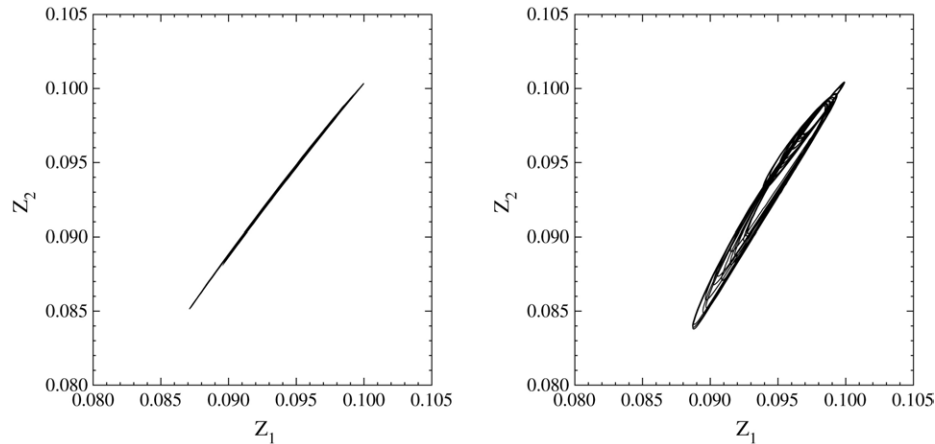


Figure 7. Predator phase plane dynamics for a two-patch system with a small stochastic variation in the respective patch closure rates,  $\text{NPZ}_{2,\neq}^I$ : (a)  $\epsilon = 0.075$  (left) and (b)  $\epsilon = 0.025$  (right). Here  $d \approx 0.142$ .

detecting this sharp transition in the dynamics can be very difficult. The values of  $\epsilon$  chosen to highlight the difference of the smooth and non-smooth collective regimes were sufficiently far apart for visually displaying the differences in the dynamics. However, as we cross the neutral normal hyperbolicity curve, the transition to non-differentiability in the invariant manifold can occur at a (subjective) computationally small scale. The concept of assessing the differentiability of generally synchronised time series was considered by Pecora *et al.* (1995); here confidence in differentiability takes the form of a simple probability, necessarily evaluated at a given spatial scale in the phase space. However, such probabilistic computations, based on a specified precision, are hard to interpret and unfortunately give no clear-cut transition associated with the loss of differentiability.

The chaotic oscillations seen in the  $\text{NPZ}^I$  model occur around  $d = 0.142$  (see Fig. 8) which intriguingly corresponds to the region around which the coupling required to guarantee normal hyperbolicity is at its lowest (see Fig. 6). This suggests that chaos could actually aid synchronisation in systems with non-identical dynamics, a possibility which we shall explore in the next section.

## 6. IMPACT OF CHAOS ON META-POPULATION DYNAMICS

Chaotic population oscillations have been observed in both theoretical ecology models and in experimental observations. Indeed, it has even been suggested that chaos is advantageous (Allen *et al.*, 1993) for the persistence of coexisting populations. Using coupled Ricker and logistic maps and both local and global noise terms, Allen *et al.* (1993) found that, over a range of diffusive coupling values, the strong oscillatory tendency of chaotic solutions indicated that extreme local

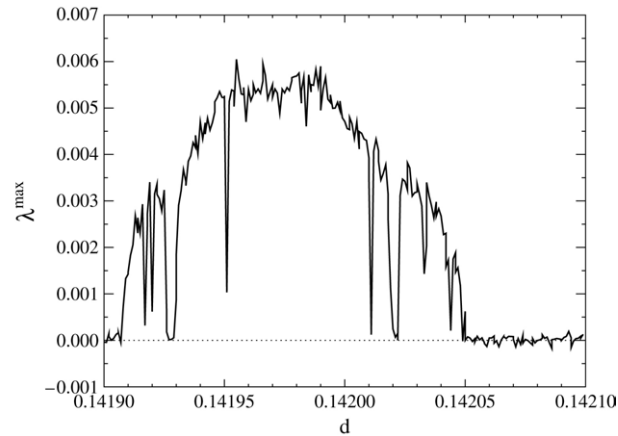


Figure 8. The maximal Lyapunov exponent of the attractor  $A$  around  $d = 0.142$  for  $\text{NPZ}^l$ . For the regions where  $\lambda_A^{\max} > 0$ ,  $A$  is chaotic. The noisy oscillation about zero is due to the fact that the calculation is merely a finite time average.

perturbation events were more likely to cause local extinction when in the chaotic regime, whereas, for global perturbations, the fact that only chaos permitted the existence of (asymptotically) unsynchronised solutions of identical oscillators in such diffusive coupling scenarios implied that global extinction was less likely as the whole lattice was unlikely to be simultaneously at a susceptible population minimum. Hence, global survival was most probable in the chaotic regime of parameter space, at least for the example systems employed. For clarity, we state that neither [Allen \*et al.\* \(1993\)](#) nor this work addresses the possibility of multi-stable synchronous solutions or the coexistence of synchronous and non-synchronous solutions. If we did have such possibilities then statements about the synchronising nature of the system would be relevant only in the context of initial conditions inside the appropriate basin of attraction. Furthermore, [Allen \*et al.\* \(1993\)](#) only considered patch systems whose individual dynamics were identical, and did not address the possibility of local variations.

In this paper, we have allowed for local parameter variations and have demonstrated how one may calculate the boundary of the region where the collective dynamics lose their differentiability. This smooth relationship often takes the form of phase synchronisation and has been observed with field data (the Canadian Hare–Lynx cycle for example). For  $\text{NPZ}_{2,\neq}^l$ , the area around the chaotic regime ([Fig. 8](#)) seems to facilitate the formation of a smooth relationship between the patch dynamics because the coupling required for this to happen ([Fig. 6](#)) is at its lowest. To see whether this is an isolated result, we compute the neutral normal hyperbolicity curve as in [Fig. 6](#), but for the case of a coupled NPZ system, with quadratic closure terms,  $\text{NPZ}_{2,\neq}^q$ . The single-patch system,  $\text{NPZ}^q$ , exhibits a small region of chaos for a closure rate of  $d \approx 0.5$  [see [Fig. 9](#) and [Edwards and Bees \(2001\)](#) for the other default parameter values]. [Fig. 10](#) presents the coupling strength required

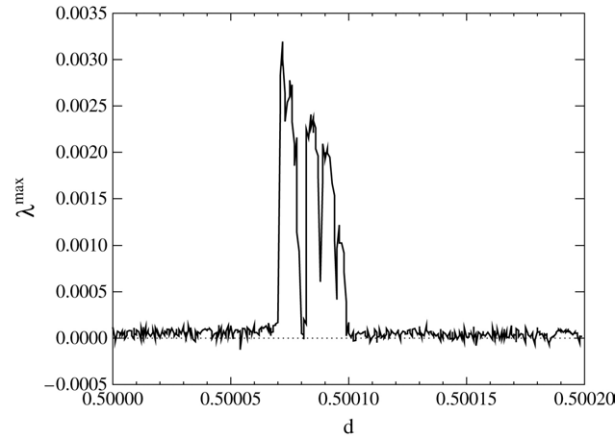


Figure 9. The maximal Lyapunov exponent of the attractor  $A$  around  $d \approx 0.5$  for the quadratic closure model,  $\text{NPZ}^q$ . For the regions where  $\lambda_A^{\max} > 0$ ,  $A$  is chaotic. The noisy oscillation about zero is due to the fact that the calculation is merely a finite time average.

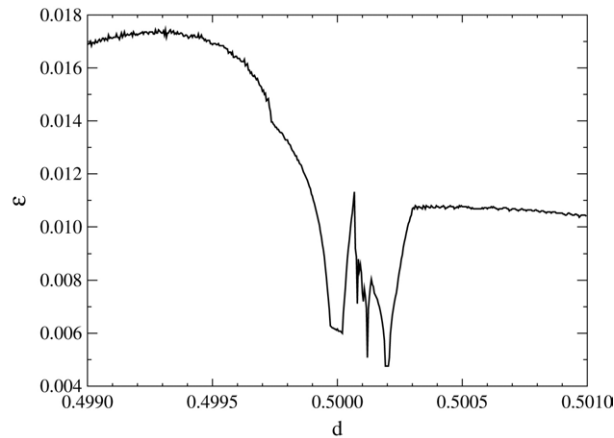


Figure 10. The neutral normal hyperbolicity curve in  $(d, \epsilon)$  space for the quadratic closure model,  $\text{NPZ}_{2, \neq}^q$ . The lack of resolution in the vertical direction is due to numerical constraints.

for the existence of a smooth inter-patch relationship against the closure rate  $d$ . As in the linear closure model,  $\text{NPZ}_{2, \neq}^l$ , the coupling strength needed for smooth generalised synchronisation decreases around the regime of chaotic oscillations. From these limited results (and similar results not presented), we hypothesise that chaotic oscillations can aid the formation of a differentiable relationship between the non-identical patch dynamics, perhaps leading to increased susceptibility to global extinction.

Of course, one should wonder why this is the case. Such behaviour has not been observed in coupled chaotic Rössler systems, suggesting that it might be an isolated result. However, we propose that it is not an isolated result, but that it is

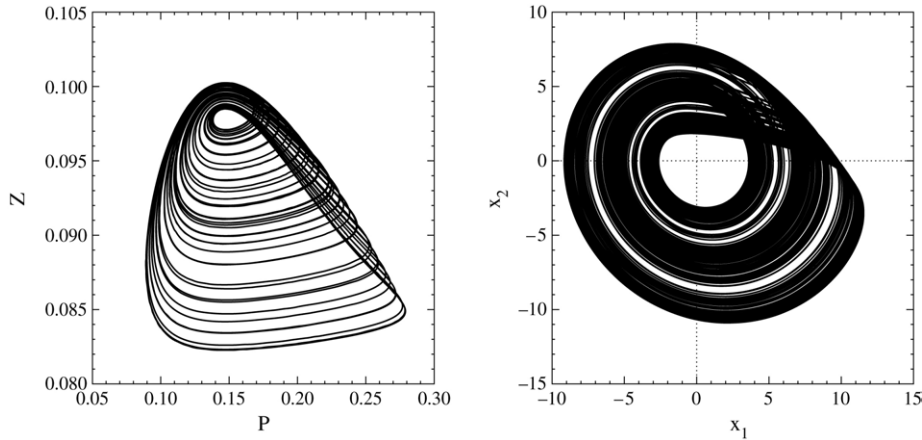


Figure 11. The chaotic attractor for the  $NPZ^I$  system (left), in  $(P, Z)$  space; on the right, the chaotic attractor for our driving Rössler system, in  $(x_1, x_2)$  space. The attractor on the left is a so-called ‘funnel’ attractor; the Rössler attractor on the right is a uniform phase chaotic attractor (UPCA).

dependent on the form of the chaotic attractor employed; which may also explain its absence in coupled Rössler systems. In Fig. 11, we plot the chaotic attractors for the example  $NPZ^I$  system, and for the Rössler system used in  $NPZ_2^I$  [Röss.]. For the  $NPZ^I$  system a ‘funnel’ attractor (Blasius and Stone, 2000a) is obtained, whereas for the Rössler system the attractor is a uniform phase chaotic attractor (UPCA). We claim that this is the crucial factor responsible for the manifestation or not of the above phenomenon.

Consider the restriction of the dynamics of both attractors to a prescribed set of Poincaré sections, and the associated return times of the chaotic orbits. Let us first introduce some simple, but necessary terminology. We shall deal with not just chaotic orbits, but also the orbits involved in the period-doubling cascade to the chaotic solution. With this in mind, the general orbit on some specified attractor  $\varphi^p(t)$ , where  $p \in \mathbb{N}$ , represents the orbit with period  $p$ . The set of times of return to a particular Poincaré section  $\Sigma$ , given by  $\Gamma = \{t_1, \dots, t_p\}$ , are the smallest such times where, given  $\varphi^p(t_0) \in \Sigma$ , if  $\varphi^p(t_i) \in \Sigma$  then  $\varphi^p(t_i + t_{i+1}) \in \Sigma$ ,  $i = 0, \dots, p - 1$ . Essential to the following argument is that we can quantify the amount of phase disparity in the various different orbits; that is, the amount of variation in these first return times. We use the following simple measure: given our set of return times, we define the parameter  $\tau = t_{\min}/t_{\max}$ , where  $t_{\min} = \min \Gamma$  etc. Consequently,  $\tau \in [0, 1]$ , and if there is low phase disparity in the orbit  $\varphi^p(t)$  then  $\tau \approx 1$ , and high phase disparity means  $\tau \approx 0$ . Note that, for period-1 orbits,  $\tau = 1$  as only one phase is present. In an obvious way we extend these definitions to chaotic orbits, although note the finite times of the simulations.

To demonstrate the differences in the phase disparity of both the funnel and UPCA attractors, Fig. 12 plots the phase disparity,  $\tau$ , against the

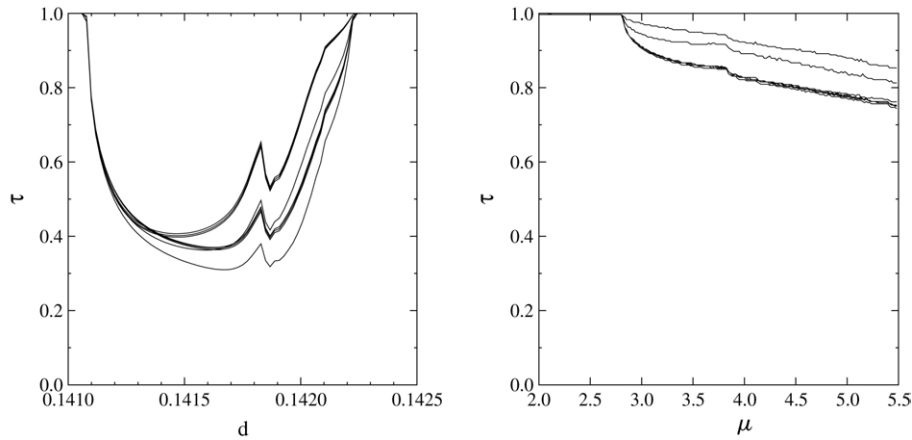


Figure 12. Phase disparity,  $\tau$ , for the NPZ<sup>l</sup> system (left), in terms of the closure rate,  $d$ ; for the Rössler system (right), in terms of the usual bifurcation parameter,  $\mu$ . For the funnel attractor case (left), there is high variation in  $\tau$  as we go through the period-doubling cascade to chaos and back again; for the UPCA case (right), there is comparatively little variation in  $\tau$  as we go from a period-1 orbit, through the usual cascade to chaos, and back to a simple period-2 orbit.

relevant bifurcation parameters, for the NPZ<sup>l</sup> and Rössler systems, using eight different, equally spaced Poincaré sections for each attractor. For the funnel attractor case, there is high variation in  $\tau$  as we proceed through a period-doubling cascade. This is due to the nature of the formation of funnel attractors; they do not form neatly around low period orbits as in the UPCA case. For the UPCA case in Fig. 12, the phase disparity shows relatively little variation all the way through a period-doubling cascade and back to a period-2 orbit.

For low period orbits in a funnel regime, a small change in the parameters can illicit a large change in the phase of the orbits. For two coupled systems, with small differences in their parameters, there can be large differences in their respective phases. As the period of the orbit increases, the number of nearby phases in the coupled oscillators increases. After the emergence of the period-2 orbit in Fig. 12 at around  $d = 0.141$ , there is a fairly high level of phase disparity in the NPZ<sup>l</sup> system, in contrast to the Rössler case (after the period-2 emergence at  $\mu \approx 2.8$ ). On reaching the chaotic funnel state, each NPZ<sup>l</sup> system has acquired a broad spectrum of return times which are likely to overlap, suggesting that strong coupling in NPZ<sub>2,≠</sub><sup>l</sup> will not be required for phase synchronisation. For the UPCA regime, there is no major change in the low phase disparity as we ascend the periods of the orbits. The spectrum of return times is already narrow ( $\tau \approx 1$ ) and there is no coupling advantage from chaos as both low and high period orbits already possess strong phase similarity. This, we hypothesise, is the mechanism for chaos aiding synchronisation in the funnel NPZ system, and the reason that it has not been observed in the UPCA Rössler system.

## 7. DISCUSSION

There is an increasing amount of evidence, from both theoretical studies and empirical observations, for coherent (synchronised) dynamical behaviour in patchy ecosystems (Grenfell *et al.*, 1998; Fox *et al.*, 2002), even when the populations seem to be evolving chaotically (Blasius and Stone, 2000a). As a prototypical example of a coupled, patchy ecosystem, we considered arbitrarily many coupled three-species models for the population dynamics of nitrogen, phytoplankton and zooplankton (a so-called NPZ model). This particular model serves well as a generic resource–prey–predator model as it exhibits a variety of dynamical behaviours, from stable equilibria to limit cycles to chaos (Steele and Henderson, 1981; Edwards and Bees, 2001).

Initially, we considered the case where the equations governing the individual patch dynamics were identical and solutions evolved chaotically. Examples were given of the non-linear mechanisms which cause the synchronisation of the individual patch dynamics. For clarity, two distinct scenarios were considered: indirect patch coupling arising from external forcing effects (such as the climate) and direct patch coupling arising from factors such as migration and/or mixing. As has been observed experimentally, if the external forcing is sufficiently strong, the patch populations will synchronise, even though they may exert no explicit effect on each other. Also, explicit patch coupling factors such as migration can force chaotically evolving populations to become synchronised.

This leads to the question of how one may be able to elucidate which mechanism is acting. For example, in Fox *et al.* (2002), there is deemed to be a statistically significant correlation between the time series of newly recruited plaice and historical temperature levels, but there is also strong evidence for significant mixing of the maturing populations of plaice around the British Isles (Dunn and Pawson, 2002). From a theoretical viewpoint, we highlight a possible method for distinguishing between the synchronising mechanisms, although the method may be hard to implement in practice. Contrary to the results on synchronisation of directly coupled patch models (Sections 3 and 5), the value of the coupling required for synchronisation of indirectly coupled patches is independent of the number of response systems (patches; Section 4). By adding an extra patch to a system and evaluating the effect (or lack of an effect) this has on the system, one may attempt to ascertain the mechanism at work. We must stress, however, that this idea applies *only* to identically coupled systems (via a blowout bifurcation); the dependence of the critical coupling on the number of patches is not necessarily observed when allowing for local parameter variations.

In practice, it is very unlikely that the equations of the governing patch dynamics will be identical. This scenario leads to a much richer array of collective behaviour, in theoretical models (Pikovsky *et al.*, 1997) and biological studies (Keith, 1963; Blasius and Stone, 2000a); such systems exhibit a more relaxed type of synchronous behaviour termed *generalised synchronisation*. This can take the

form of phase/anti-phase synchronisation or other forms of complex, yet deterministic, collective behaviour. It was demonstrated how one can compute the boundary across which this inter-patch functional relationship loses its smoothness. Examples were given of the difference in the subsequent dynamics, after this smoothness is lost. This analysis yielded an initially curious result: the patch dynamics formed a smooth collective relationship most easily (i.e., required the smallest coupling strength) in the chaotic regime. The effect was seen in both NPZ systems with linear and quadratic closure terms.

This result for directly coupled patch systems, with local parameter variations, leads to conclusions which are in stark contrast to those of [Allen \*et al.\* \(1993\)](#) with regard to the role of chaos in directly coupled identical patch systems. When allowing for such local variations, our results suggest that certain types of chaos can in fact enhance the ability of the system to form a strong collective relationship (such as phase synchronisation). This phenomenon increases the potential of global extinction for the following reason. For these particular chaotic regimes, over a range of coupling values, the system is more likely to be in a state of smooth generalised synchronisation—specifically phase synchronisation. So, while the amplitudes of the patch oscillations are different, any population maxima and minima occur at the same time throughout the whole lattice. This means that any global perturbation has a higher likelihood of causing a global extinction as all the patch inhabitants reach their respective population minima at the same time. This is precisely the same argument as applied to non-chaotic dynamics ([Allen \*et al.\*, 1993](#)).

The increased predisposition for non-identical patches with chaotic dynamics to synchronise in the test-case systems presented here strongly suggests a link to the type of chaotic attractor involved. The NPZ chaotic attractors are of the funnel class. We showed that, compared to the case for a previously well studied Rössler UPCA (uniform phase chaotic attractor) system, the structural sensitivity in the phases of the periodic orbits, which occur in the period-doubling cascade to funnel-type chaos, intimates that synchronising close—yet non-identical—oscillators takes less coupling strength as the chaotic state is ultimately approached through period doubling. This phase sensitivity is not present in the UPCA Rössler system, explaining why this phenomenon was not observed in such a system before. We suggest that we have merely touched upon the true complexity of this topic: the calculation of the normal hyperbolicity curve, from which this phenomenon became apparent, is closely linked to the most negative Lyapunov exponents in the underlying dynamics which would require a thorough exploration in relation to the phases of periodic orbits.

Recent developments in non-linear dynamics are helping to unravel some of the mechanisms at work in more complex ecosystems. In this paper, we have presented some of the various modes of population synchrony in non-linear, possibly chaotically evolving patchy ecosystems, with reference to both observed phenomena and new evidence that the true role of chaos in interacting ecosystems is more complex than expected.

## ACKNOWLEDGEMENTS

RMH is grateful for an EPSRC research studentship; the authors would like to thank two anonymous referees for helpful comments and suggestions.

## APPENDIX A: GENERALISED SYNCHRONISATION

Here, we list the full set of conditions on the generalised synchronisation relation,  $\phi$ . The function  $\phi$  must be independent of the initial conditions of the response system,  $\mathbf{s}(0)$ , as long as they are inside the basin of attraction of the generally synchronised attractor. The existence of  $\phi$  is only required *after transients have decayed*. In Abarbanel *et al.* (1996), the following properties of  $\phi$  are laid down:

- (1)  $\phi$  has no explicit time dependence.
- (2) Points in  $E$  space are mapped to *points* in  $S$  space. The function  $\phi$  need not be injective and consequently not be invertible but has a finite number of branches (with some rule for moving from branch to branch).
- (3) On each branch,  $\phi$  is locally continuous.

## APPENDIX B: PROOF THAT STABLE GENERALISED SYNCHRONISATION IS EQUIVALENT TO STABLE SYNCHRONISATION IN THE DRIVE-RESPONSE SYSTEM

Abarbanel *et al.* (1996) described but did not formally prove this equivalence; it was observed that the linear evolutions of the two stability problems were identical. For completeness, we formalise this approach as it additionally requires smoothness conditions in the underlying dynamics. To prove that stable generalised synchronisation  $\Leftrightarrow$  stable synchronisation in (1), first consider the linear evolution operators for the variables  $\xi_i(t) = \mathbf{s}_i(t) - \phi(\mathbf{E}(t))$  and  $\xi_{ij}(t) = \mathbf{s}_i(t) - \mathbf{s}_j(t)$  denoted by  $\Lambda_i(t)$  and  $\Lambda_{i,j}(t)$ , respectively. Using a different definition for the Lyapunov exponents (Eckmann and Ruelle, 1985), the stability of the generally synchronised motions is determined by the logarithms of the limiting eigenvalues,  $\log(\mu_i)$ , of the matrix:

$$\lim_{t \rightarrow \infty} ((\Lambda_i(t))^\dagger \Lambda_i(t))^{\frac{1}{2t}}, \quad (\text{B.1})$$

where  $\dagger$  denotes the adjoint of the operator.

Analogously, the stability of the synchronised motions is governed by the logarithms of the limiting eigenvalues,  $\log(\mu_{i,j})$ , of the matrix:

$$\lim_{t \rightarrow \infty} ((\Lambda_{i,j}(t))^\dagger \Lambda_{i,j}(t))^{\frac{1}{2t}}. \quad (\text{B.2})$$

If all the  $\log(\mu_i) < 0$  and the  $\log(\mu_{i,j}) < 0$ , then both the generally synchronised and the fully synchronised systems will be linearly stable. If just one of the  $\log(\mu_i) > 0$  and one of the  $\log(\mu_{i,j}) > 0$  then the respective systems will be linearly unstable. However, both  $\Lambda_i(t)$  and  $\Lambda_{i,j}(t)$  satisfy the following ODE:

$$\begin{aligned}\frac{d\Lambda_*(t)}{dt} &= DG^t(\phi(\mathbf{E}), \Theta, \mathbf{E})\Lambda_*(t), \\ \Lambda_*(0) &= \mathbf{I}_m,\end{aligned}\tag{B.3}$$

where  $\mathbf{I}_m$  is the  $m$ -dimensional identity matrix and the index  $*$  =  $i$  or  $i, j$ . The matrix  $DG^t(\phi(\mathbf{E}), \Theta, \mathbf{E})$  is simply the Jacobian of the response system dynamics, defined by the function  $\mathbf{G}(\cdot)$ , evaluated at time  $t$  for the generally synchronised solution,  $\phi(\mathbf{E})$ . Now, we first note that  $DG^t(\phi(\mathbf{E}), \Theta, \mathbf{E})$  is  $C^0(\mathbb{R}^m)$ , because  $\mathbf{G}(\cdot)$  is assumed to be  $C^1(\mathbb{R}^m)$ . Coupled with the fact that  $\Lambda_i(0) = \Lambda_{i,j}(0)$ , we must have that  $\Lambda_i(t)$  and  $\Lambda_{i,j}(t)$  are in fact the same operators on  $C^1(\mathbb{R}^m)$ , due to the existence and uniqueness of the solution of an initial value problem such as this. Finally, because they are the same operators,  $\log(\mu_i) \equiv \log(\mu_{i,j})$  and we must have that the generally synchronised solution is stable/unstable iff the fully synchronised solution is stable/unstable.

## REFERENCES

- Abarbanel, H. D. I., N. F. Rulkov and M. M. Sushchik (1996). Generalized synchronization of chaos: the auxiliary systems approach. *Phys. Rev. E* **53**, 4258–4535.
- Alexander, J. C., J. A. Yorke, Z. You and I. Kan (1992). Riddled basins. *Int. J. Bifurcation Chaos* **2**, 795–813.
- Allen, J., W. Schaffer and D. Rosko (1993). Chaos reduces species extinction by amplifying local population noise. *Nature* **364**, 229–234.
- Ashwin, P., J. Buescu and I. Stewart (1994). Bubbling of attractors and synchronisation of chaotic oscillators. *Phys. Lett. A* **193**, 126–139.
- Belykh, B., I. V. Belykh and E. Mosekilde (2001). Cluster synchronization modes in an ensemble of coupled chaotic oscillators. *Phys. Rev. E* **63**, 036216.
- Blasius, B. and L. Stone (2000a). Chaos and phase synchronization in ecological systems. *Int. J. Bifurcation Chaos* **10**, 2361–2380.
- Blasius, B. and L. Stone (2000b). Nonlinearity and the Moran effect. *Nature* **406**, 846–847.
- Dunn, M. R. and M. G. Pawson (2002). The stock structure and migrations of plaice populations on the west coast of England and Wales. *J. Fish Biol.* **61**, 360–393.
- Eckmann, J.-P. and D. Ruelle (1985). Ergodic theory of chaos and strange attractors. *Rev. Mod. Phys.* **57**, 617–656.
- Edwards, A. M. and M. A. Bees (2001). Generic dynamics of a simple plankton population model with a non-integer exponent of closure. *Chaos Solitons Fractals* **12**, 289–300.
- Edwards, A. M. and J. Brindley (1996). Oscillatory behaviour in a three component plankton population model. *Dyn. Stab. Syst.* **11**, 347–370.

- Fox, C. J., B. P. Planque and C. P. Darby (2002). Synchrony in the recruitment time-series of plaice (*Pleuronectes platessa* L) around the United Kingdom and the influence of sea temperature. *J. Sea. Res.* **44**, 159–168.
- Fujisaka, H. and T. Yamada (1983). Stability theory of synchronized motion in coupled-oscillator systems. *Prog. Theor. Phys.* **69**, 32–48.
- Grenfell, B. T., K. Wilson, B. F. Finkelstädt, T. N. Coulson, S. Murray, S. D. Albon, J. M. Pemberton, T. H. Clutton-Brock and M. J. Crawley (1998). Noise and determinism in synchronized sheep dynamics. *Nature* **394**, 674–677.
- Hastings, A. and T. Powell (1991). Chaos in a three species food chain. *Ecology* **72**, 896–903.
- Hillary, R. M. (2003). Effects of turbulence and a patchy environment on the dynamics of plankton populations, PhD thesis, University of Surrey.
- Hillary, R. M. and M. A. Bees (2004). Plankton lattices and the role of chaos in plankton patchiness. *Phys. Rev. E* **69**, 031913.
- Hudson, P. J. and I. M. Cattadori (1999). The Moran effect: a cause of population synchrony. *TREE* **14**, 1–2.
- Josic, K. (1998). Invariant manifolds and synchronization of coupled dynamical systems. *Phys. Rev. Lett.* **80**, 3053–3056.
- Keith, L. B. (1963). *Wildlife's Ten Year Cycle*, Cambridge: Cambridge University Press.
- Moran, P. A. P. (1953). The statistical analysis of the Canadian lynx cycle. *Aust. J. Zool.* **1**, 291–298.
- Ott, E. and J. C. Sommerer (1994). Blowout bifurcations: the occurrence of riddled basins and on–off intermittency. *Phys. Lett. A* **188**, 39–47.
- Pecora, L. M. (1998). Synchronization conditions and desynchronizing patterns in coupled limit-cycle and chaotic systems. *Phys. Rev. E* **58**, 347–360.
- Pecora, L. M. and T. L. Carroll (1990). Synchronization in chaotic systems. *Phys. Rev. Lett.* **64**, 821–825.
- Pecora, L. M., T. L. Carroll and J. F. Heagy (1995). Statistics for mathematical properties of maps between time series embeddings. *Phys. Rev. E* **52**, 3420–3439.
- Pikovsky, A. S. (1984). On the interaction of strange attractors. *Z. Phys. B* **55**, 149–154.
- Pikovsky, A. S., M. G. Rosenblum, J. V. Osipov and J. Kurths (1997). Phase synchronization of chaotic oscillators by external driving. *Physica D* **104**, 219–238.
- Rössler, O. E. (1976). An equation for continuous chaos. *Phys. Lett. A* **57**, 397–398.
- Steele, J. H. and E. W. Henderson (1981). A simple plankton model. *Am. Naturalist* **117**, 157–183.
- Sugihara, G. and R. M. May (1990). Non-linear forecasting as a way of distinguishing chaos from measurement error. *Nature* **344**, 734–741.
- Wiggins, S. (1994). *Normally Hyperbolic Invariant Manifolds in Dynamical Systems*, Springer: New York.

Received 13 October 2003 and accepted 20 May 2004